Subaqueous barchan dunes in turbulent shear flow. Part 2: Fluid flow

By F. CHARRU AND E.M. FRANKLIN

Institut de Mécanique des Fluides de Toulouse - CNRS–Université de Toulouse - Allée C. Soula, 31400 Toulouse, France

(Received ?? and in revised form ??)

We report an experimental study of the turbulent flow above a barchan dune in a channel, from PIV measurements. Particular attention is paid to the assessment of the asymptotic theory of Hunt, Leibovich and Richards (1988). From the evaluation of the Lagrangian speed-up and Reynolds stresses, the existence of a two-layer structure –an essentially inviscid outer layer and a viscous (turbulent) inner layer– is confirmed. The present flow however exhibits particular features, related to its nature (a channel flow, not a boundary layer), and the importance of viscosity effects in the inner layer (Reynolds number effect). The speed-up is found to increase along the dune up to the brink, whereas the turbulent stresses decrease. The total shear stress at the dune surface, including the viscous part, increases, up to twice its value on the smooth wall. These results are found to be weakly dependent on Reynolds number. The implications of these results on the dune motion, which was presented in the Part One of this study, are finally discussed.

1. Introduction

1.1. *Aim of the paper*

The question of the flow over a bump, hill or dune, or over a wavy surface, raises fondamental issues such as the structure of the flow and the distribution of velocity and stresses. This question has numerous applications in meteorology and oceanography (Taylor, Mason & Bradley 1987; Belcher & Hunt 1998), such as soil erosion and dune motion. The presence of a bump in a boundary-layer flow introduces new scales to the problem of the flow above a flat ground, first of all the length L (or wavelength) and height H of the bump. Many studies, experimental, numerical and theoretical, have been devoted to the analysis of the perturbed flow. Fruitful insights have been provided, in particular, by asymptotic analyses exploiting the layered structure of the flow, which are shortly reviewed below.

Another field of application is sand or particle transport in pipes or channels (*e.g.* in petroleum engineering or food industry), where the particles form an irregular bed on the bottom wall sheared by the fluid flow. This kind of closed flow has received less attention than large-scale open flows. It may differ in several respects, such that (i) the dune size is not small in comparison with the channel width or the pipe diameter so that confinement effects can be expected; (ii) the flow is rotational over the entire depth, *i.e.* there is no region of potential flow; (iii) the Reynolds number is generally smaller than in open flows so that viscous effects may be of importance; (iv) the flow regime may change from smooth, over the channel wall, to rough, over the dune, which situation is opposite to that encountered for deserts dunes where the sand roughness is smaller than that of the pebbly surrounding ground. In the first part of this study (Franklin & Charru 2011),

experiments were reported on the formation and migration of isolated dunes in a closed channel. In the present second part, the fluid flow above these dunes is investigated, with particular emphasis on the assessment of a layered structure, the stresses at the dune surface, and Reynolds number effects.

The paper is organized as follows. The theoretical background and available experimental results are first presented. The experimental apparatus used in the present study is briefly described in §2, along with some preliminary observations. The mean flow is analysed in §3 and the relevance of the distinction between two layers is discussed. Stresses are studied in §4, with particular emphasis on the shear stress at the dune surface. The Reynolds number effect is investigated in §5. A final discussion is given in the last Section.

1.2. *Background*

Asymptotic analyses of the perturbed flow over a bump are essentially based on the governing equations linearized for small slope H/L. Within this frame, the basic problem is that of the flow over a sinusoidal bottom, the more general flow over a bump of given profile being then obtained from inverse Fourier transforms. Such analyses cannot account for flow separation on the leeward side of bumps, which can be analyzed using the triple-deck theory (see *e.g.* Schlichting & Gersten 2000).

The laminar flow problem has been first solved by Benjamin (1959), with particular emphasis on the stresses on the (possibly moving) bottom, in the context of the generation of water waves by the wind. Benjamin's analysis accounts for the common situation where the wave amplitude is not small compared to the characteristic length of variation of the velocity in the transverse direction (*e.g.* the thickness of a boundary layer). This was made possible thanks to the use of an orthogonal curvilinear system of coordinates with which the two-dimensional equations for the flow above a sinusoidal bottom finally reduce to the steady Orr-Sommerfeld equation. Benjamin's analysis is based on the fact that far from the wall, viscous effects are negligible and the Orr-Sommerfeld equation reduces to the Rayleigh equation, whose solution gives the pressure distribution close to the wall. Within a thin 'wall friction layer', viscous effects must be taken into account while the curvature of the base velocity profile can be neglected. Benjamin considered several unperturbed base flow, including the logarithmic mean velocity profile of a turbulent boundary layer. Regarding the phase of the shear stress on a fixed wavy bottom, a quantity of major importance when the bottom is erodible (Luchini & Charru 2010), Benjamin found that it leads that of the bottom so that the maximum shear stress is reached upstream of the crest of the bottom deformation; in particular, for a single symmetric bump of the form $(1+(x/L)^2)^{-1}$, the maximum shear stress is located at a distance $x/L \approx 0.24$ upstream of the crest.

The analysis of Jackson and Hunt (1975) extends that of Benjamin (1959) to turbulent flow, with the same idea that the perturbed flow over the bump has a two-layer structure: an inviscid outer layer, and an inner layer governed by the boundary layer equations. In the latter, turbulence is at equilibrium so that the Reynolds shear stress can be modelled with the mixing length theory. The thickness δ_i of the inner layer can be derived from the balance of the longitudinal acceleration and the stress gradient; for logarithmic unperturbed velocity profile, $U_0 = (u_*/\kappa)\ln(y/y_0)$ where y_0 is the hydrodynamic roughness, it is given by

$$(\delta_i/L)\ln(\delta_i/y_0) = 2\kappa^2. \tag{1.1}$$

The theory of Jackson and Hunt was then improved and generalized in several ways, notably by Sykes (1980) and Hunt, Leibovich and Richards (1988), see the review by Belcher and Hunt (1998). Hunt *et al.* (1988) introduced an intermediate (or middle)

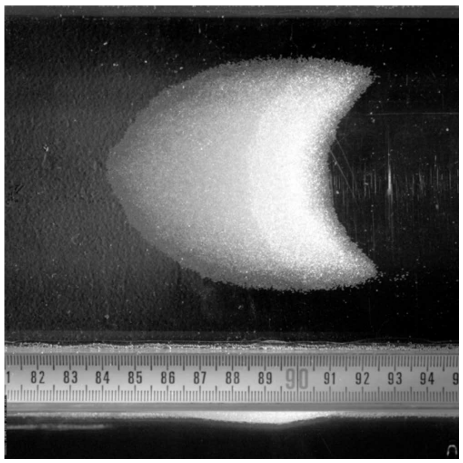

FIGURE 1. Subaqueous barchan dune, top view (above the ruler) and side view (below) seen from an inclined mirror, from the present experiments. The water flows from left to right.

layer in order to ensure continuity of the longitudinal velocity. In this middle layer, the dynamics of the perturbation is still inviscid but rotational, and the vertical pressure gradient $\partial_y p$ is assumed to be negligible. For long hills, *i.e.* $L > \delta_{\rm BL}$ where $\delta_{\rm BL}$ is the thickness of the boundary layer of the undisturbed upstream flow, the boundary between the upper and middle layers is located at the displaced height $\delta_m = \delta_{\rm BL}$ above the hill; for shorter hills, $\delta_m = L \ln^{-1/2}(L/y_0)$. More details are given in the Appendix. The asymptotic analyses of Hunt *et al.* (1988) have been widely used in models for aeolian sand dunes (Weng *et al.* 1991; Kroy, Sauermann & Hermann 2002; Andreotti, Claudin & Douady 2002).

Field observations have validated the above analyses, see the review by Taylor, Mason and Bradley (1987), although accurate comparison is hardly possible because of the scarcity of the measurements. Laboratary experiments allow more thorough investigation, but most of them consider periodic wavy walls: Abrams and Hanratty (1985) discuss the relevance of turbulence models and their ability to predict the wall shear stress; Gong, Taylor & Dörnbrack (1996) study roughness effects and secondary flows, and the ability of large-eddy simulation to reproduce these secondary flows; Poggi, Katul, Albertson & Ridolfi (2007) discuss the validity of Jackson & Hunt's theory. The flow above isolated dunes has received much less attention.

2. Experimental apparatus and first observations

2.1. *Apparatus*

The experimental apparatus is the same as that presented in (Franklin & Charru, 2011), so that its description is only briefly skecthed here. It mainly consists of a horizontal plexiglass channel, six meters long, with rectangular cross-section of height $2\delta = 60$ mm and width $b = 120$ mm (Figure 2). Small conical heaps of particles were formed in the channel by dropping the particles from a small hole in the upper wall located at 4.15 m form the entrance of the channel. Then the flow was started up, and the heap quickly deformed into a barchan dune.

The bulk velocity U_b of the flow, defined as the ratio of the measured volumetric flow rate and the channel cross-section, was varied between 0.15 and 0.4 $\mathrm{m\,s^{-1}}$. The

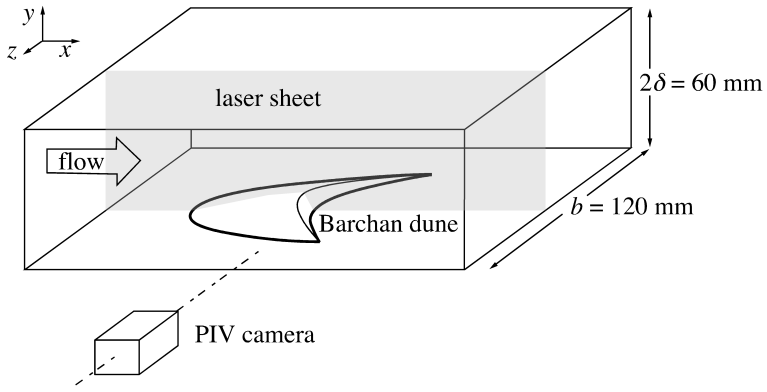

FIGURE 2. Sketch of the experimental set-up and a barchan dune.

corresponding Reynolds number

$$Re = \frac{U_b\, 2\delta}{\nu} \tag{2.1}$$

was in the range $9000 - 24000$.

As shown in Part One, in the last third of the channel, the water flow has the classical features of a fully-developed turbulent channel flow. The mean flow velocity $U_0(y)$ is well represented by the classical log law, $U_0^+ = (1/\kappa)\ln y^+ + B$ in wall units, for y^+ in the range 30–200 ($2 \lesssim y\,(\mathrm{mm}) \lesssim 10$), with the von Kármán coefficient $\kappa = 0.41$ and the additive constant $B = 5.5$ having their usual values (Davidson 2004). The shear velocity u_*, as determined by curve fitting, was found to agree with that predicted by the Blasius correlation

$$c_f = \frac{u_*^2}{\frac{1}{2}U_b^2} = 0.079\,(1.33\,Re)^{-1/4}, \tag{2.2}$$

where $1.33\,Re$ is the Reynolds number based on the hydraulic diameter of the rectangular channel. The whole velocity profile, from the lower wall ($y = 0$) up to the centerline ($y = \delta$), was found to be nicely fitted by adding to the log law two usual corrections: the Spalding's correction near the wall and the Coles-Lewkowicz' law of the wake in the center part of the channel (Panton 2007). In particular, the measurements and the above fit gave nearly the same maximum velocity at the centerline, $U_\delta = U_0(\delta) \approx 1.19\,U_b$, with maximum difference less than 2% in the explored range of Reynolds number. Reynolds stresses were also shown to have their usual values, with nearly constant shear stress $-\overline{u'v'}$, close to u_*^2, in the region $30 < y^+ < 200$ where the log-law holds.

2.2. *Velocity measurements above the dune*

For the mean flow to be as close as possible to stationary in the fixed reference frame of the camera, the dune velocity had to be as small as possible, which lead to choose heavy zircone particles with median diameter 0.19 mm and density $\rho_p = 3760\ \mathrm{kg\,m^{-3}}$ (those of Series 4 used in Part One). The settling velocity of these particles is $V_{\mathrm{fall}} = 35\ \mathrm{mm\,s^{-1}}$, and their settling Reynolds number, $Re_{\mathrm{fall}} = 6.6$. For the largest fluid flow rate, the particle Reynolds number was $Re_p = u_* d/\nu = 4.0$. The choice of the dune size had to meet two opposite requirements: it must be sufficiently large to induce significant perturbations of the fluid flow, and sufficiently small to keep the dune in the logarithmic region and ensure small confinement effect of the upper and lateral walls. The corresponding length and height were typically $L = 40$ mm and $H = 5$ mm, this height corresponding to one-third, at most, of the thickness of the logarithmic layer.

Fluid velocity measurements were performed using Particle Image Velocimetry (PIV) and images were processed with the software PIVIS developed at IMFT, see Part One for details. Once a barchan dune had formed from the initial heap of particles, the laser sheet was positioned in the vertical symmetry plane of the dune (which might be slighly different from the symmetry plane of the channel), as shown in Figure 2. The field of view was covering either the whole dune and channel height, or a smaller area for better spatial resolution. For most of the figures presented here, this field was 22×17 mm^2, corresponding to a spatial resolution of the velocity field of 0.14 mm in both directions (with correlation boxes of 16×16 pixels and overlap of 50%). Due to smudges of glue at the corners of the plexiglass channel, the fluid flow close to the lower wall was blurred up to a distance of about one millimeter, leading there to uncertain measurements which will not be reported. The time interval between the two frames of a pair ranged from 224 μs (for the highest Reynolds number) to 496 μs (for the lower one), and the frequency of the pairs was 4 Hz. The number of pairs per run ranged from 108 to 864, which was chosen such that the displacement of the dune was small during one run. This displacement was 3.5 mm for the highest Reynolds number and much less for the lower ones. The mean velocity and Reynolds stresses were obtained by averaging the instantaneous fields; convergence within 1% was achieved with a number of fields (i.e. the number of pairs of images) of about 30 for the mean velocity and 200 for the Reynolds stresses.

2.3. *Preliminary observations*

Figure 3a shows a typical instantaneous velocity field in the vertical symmetry plane of a dune, with $y = 0$ corresponding to the bottom wall and $x = 0$ to the position of the brink of the dune profile. The flow velocity $U_b = 0.184$ m s^{-1} ($Re = 9260$) is just below the threshold for particle motion, so that the dune is at rest. An enlargement of the region downstream of the slip face is displayed in Figure 3b, showing the existence of a recirculating flow; note that the base of the slip face is hidden by the horn in between the laser sheet and the camera, so that fluid may flow across the apparent dune boundary. Successive images downstream of the slip face display quite different velocity fields, showing that the recirculating flow is strongly unsteady: as soon as it is formed, a vortex detaches from the dune, another vortex then growing at the same place. The sampling frequency of the pairs of images was not high enough to provide a detailed picture of the vortex dynamics, in particular the distribution of the detachment times. In order to get a wider picture of the flow along the dune while keeping high spatial resolution, one or two more flow fields were recorded upstream or downstream of that centered on the dune brink. Most of the figures shown in the following correspond to two or three adjacent flow fields merged together.

Figure 4a shows typical vertical profiles of the time-averaged velocity in the symmetry plane of a dune, at longitudinal positions equally spaced from the dune brink ; Figure 4b displays the corresponding streamlines. It can be seen that streamlines come closer to each other along the dune, and reach their highest point slightly downstream of the brink; the detachment of the boundary layer downstream of the slip face and the mean back-flow in the wake are also clearly visible.

Figure 4b also displays a fit of the dune profile (the dashed line) with the cosine function

$$h(x) = h_M \cos \frac{\pi(x - x_0)}{2L}, \tag{2.3}$$

where $L = 35$ mm, one-fourth of the wavelength, is close to the dune length measured from the foot of the upstream face to the foot of the slip face. As discussed in Part One, (2.3) was found to provide a better fit than the bell shape $h(x) = h_M/(1 + (x -$

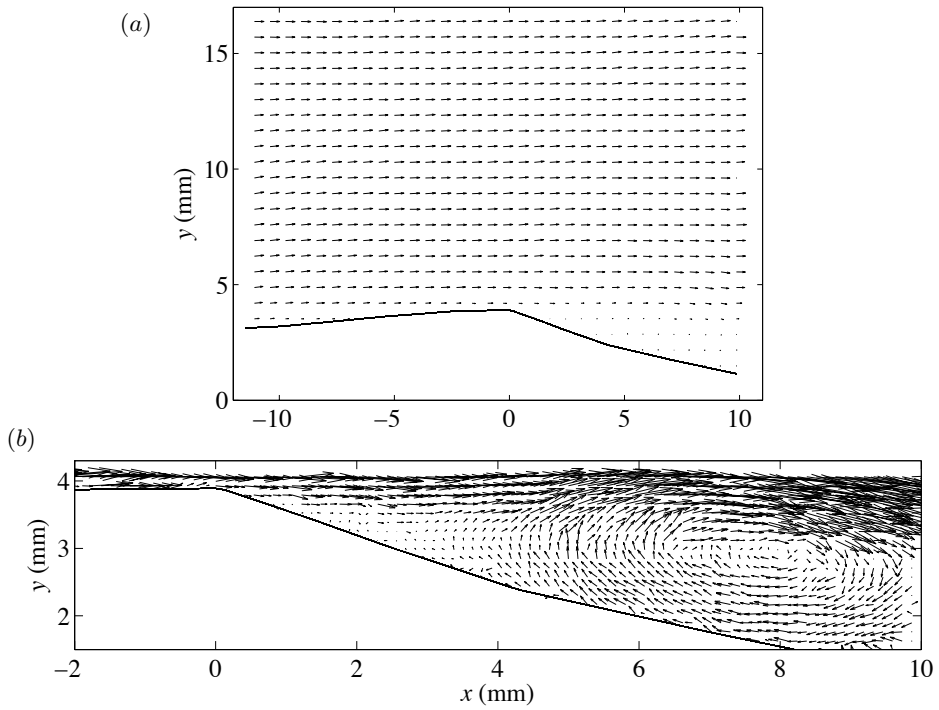

FIGURE 3. (a) Typical velocity field in the vertical symmetry plane above a dune (thick line); (b), enlargement of the region downstream of the brink. $U_\delta = 0.184\ \mathrm{m\,s^{-1}}$ ($Re = 9260$, $u_* = 9.45\ \mathrm{mm\,s^{-1}}$).

$x_0)^2/L^2$) often chosen in theoretical analyses (Benjamin 1959; Hunt *et al.* 1988), whose tail decreases too slowly. An important point here is that the dune brink does not coincide with the summit of the fit which is rather located at the distance $x \approx 4\mathrm{mm} \approx h_M$ downstream. However, the height H of the dune at the brink is hardly smaller than h_M, typically by 0.1 mm. The dune slope, defined as $(\pi/2L)h_M$, is 0.18.

3. Mean flow

3.1. *Mean velocity and speed-up*

Figure 5a displays profiles of the longitudinal velocity at five longitudinal positions upstream of the dune crest, with the vertical position $y_d = y - h(x)$ measured from the dune surface $h(x)$. This figure shows that, at a given elevation y_d above the dune, the fluid velocity increases and reaches its maximum velocity at the crest. The same plot with logarithmic vertical scale, displayed in Figure 5b, does not exhibit any clear straight line, so that the velocity departs from the logarithmic profile.

A deeper insight into the disturbed flow can be gained from the speed-up ΔU at the distance $y_d = y - h(x)$ above the dune, defined as

$$\Delta U(x, y) = U(x, y) - U_0(y_d), \tag{3.1}$$

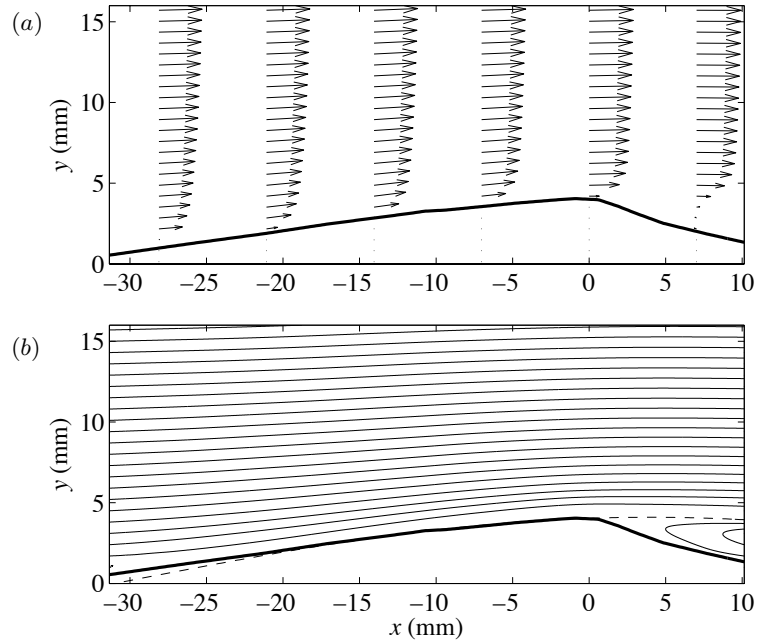

FIGURE 4. Typical mean flow above a dune, for $U_\delta = 0.184$ m s^{-1} ($Re = 9260$, $u_* = 9.45$ mm s^{-1}); (a) vertical profiles of the velocity; (b) streamlines. Dashed line : dune profile fitted by (2.3) with $h_M = 4.1$ mm, $L = 35$ mm, $x_0 = 4$ mm. The dune height at the brink is $H = 4.0$ mm.

i.e. the difference between the actual longitudinal velocity $U(x, y)$ and the unperturbed velocity $U_0(y_d)$ at the same elevation above the bottom wall, far upstream of the dune (Figure 6a). In the following, $U_0(y)$ is the logarithmic law with the wall and wake corrections, as defined in §2.1, and the friction velocity taken from the Blasius correlation (2.2). Figure 6b displays vertical profiles of the speed-up ΔU at the dune crest ($x/L = 0$) and four positions upstream ($x/L < 0$), normalized with the maximum velocity $U_\delta = U_0(\delta)$. The speed-up profile at $x/L = 0.8$ appears to be nearly flat, but a peak develops as the dune crest is approached, at the height $y_d \approx 0.02\,\delta$. The maximum of the peak is reached at the crest, with value $\Delta U \approx 0.26\,U_\delta \approx 4.3\,u_*$.

The speed-up defined above from the shifted vertical coordinate is the simplest to compute, but it does not correspond to the actual variation of the Lagrangian velocity of a fluid particle. Along any streamline $y_s(x)$ (or trajectory) above the dune, this Lagrangian speed-up is

$$\Delta U_L(x, y_s) = U(x, y_s) - U_0(y_{s0}), \tag{3.2}$$

where $U(x, y_s)$ is the measured velocity and $U_0(y_{s0})$ is the unperturbed upstream velocity on the same streamline with elevation y_{s0} above the wall. Since the spanwise velocity is zero in the symmetry plane of the dune, streamlines could be computed from the measured mean velocity field as the lines tangent everywhere to the plane vector field (as those shown in Figure 4b). However, the field of view did not extend far enough upstream for the location y_{s0} of the undisturbed streamlines to be determined accurately, so that y_{s0} had to be estimated from some extrapolation. This was done by assuming plane

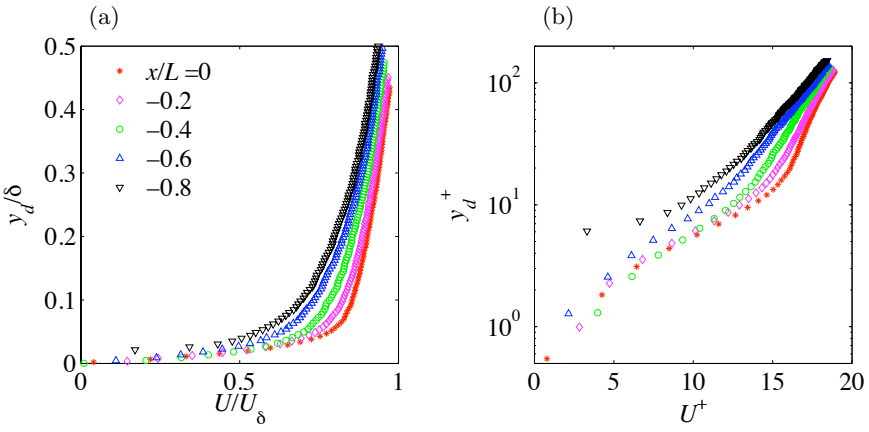

FIGURE 5. Longitudinal velocity profiles above the crest ($x/L = 0$) and four positions upstream ($x/L < 0$), with the vertical distance $y_d = y - h(x)$ measured from the dune surface; (a) linear scale, (b) log scale. The parameter values are the same as in Figure 4.

flow upstream of the field of view (*i.e.* negligible divergence of the streamlines in the horizontal plane), allowing y_{s0} to be calculated from conservation of the flow rate

$$\int_0^{y_{s0}} U_0(y)dy = \int_{h(x_u)}^{y_s} U(x_u, y)dy$$

where x_u is the upstream boundary of the field of view of the camera.

Vertical profiles of the resulting Lagrangian speed-up are displayed in Figure 6c; they are similar to those determined from the shift of the vertical coordinate, with however two differences. First, close to the crest ($x/L \gtrsim -0.5$), the speed-up is smaller by a factor of about two (because the compression of the streamlines is now accounted for), and is reached at a higher elevation above the dune, $y_d \approx 0.05\,\delta$. Second, close to the dune foot ($x/L \lesssim -0.5$), the peak disappears and the speed-up is negative near the dune surface, because of the vertical divergence of the streamlines. Note that the relative speed-up, *i.e.* the Lagrangian speed-up normalized with the unperturbed velocity $U_0(y_d)$, exhibits larger values (not shown) and reaches 40% at the crest.

Profiles of the vertical velocity $V(x, y_d)$ are shown in Figure 7. These profiles all exhibit a peak at the elevation $y_d \approx 0.05\,\delta$, above which V slowly decreases. At a given elevation above the dune, V first increases and then decreases as the crest is approached, with largest velocity at the position $x/L \approx -0.4$.

The variations along the dune of the peaks of the Lagrangian speed-up, $\Delta U_{L,\mathrm{peak}}$, and vertical velocity, V_{peak}, as well as their vertical locations, are plotted in Figure 8. It appears that $\Delta U_{L,\mathrm{peak}}$ increases linearly up to the dune crest and then decreases (Figure 8a), with a maximum of $1.3\,U_{\mathrm{ref}}$ where $U_{\mathrm{ref}} = (H/\delta)U_\delta$ is the expected order of magnitude; the distance of the peak from the dune surface slightly decreases from $0.06\,\delta$ at $x/L = -0.6$ to $0.05\,\delta$ at the crest ($x/L = 0$) (Figure 8b). The corresponding variations of V_{peak} are displayed in Figure 8c and 8d. The value of the peak increases and then decreases, with a maximum of $0.7\,V_{\mathrm{ref}}$ where $V_{\mathrm{ref}} = (H/L)U_\delta$ is the expected order of magnitude; this maximum is reached at $x/L \approx -0.4$ which corresponds to the location of the inflexion point of the streamlines. The secondary peak downstream of the crest (at $x/L \approx 0.2$) is related to the vortex in the wake of the dune.

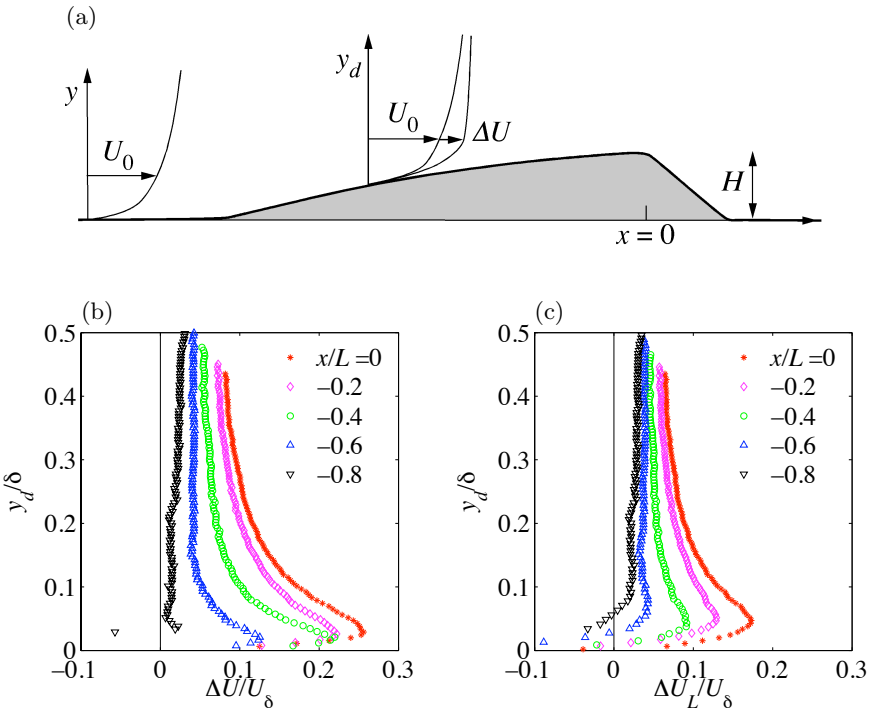

FIGURE 6. (a) Sketch of the definition of the speed-up ΔU; (b), profiles of the 'same-elevation' speed-up (3.1), normalized with U_δ, at five x-positions upstream of the crest ($x/L = 0$); (c), profiles of the Lagrangian speed-up (3.2) at the same x-positions. Parameters: see Figure 4.

3.2. *Analysis of the flow in the outer-layer*

As mentioned in the introduction, the flow over a dune or a hill with small slope is in general not fully developed, and can be considered as the superposition of two layers: an upper outer layer where the dynamics of the perturbation is essentially inviscid, and an inner layer where the perturbation shear stresses (turbulent and possibly viscous) play a significant dynamic role. The solution in the outer layer provides in particular the pressure $P(x)$ which drives the flow in the inner layer.

The thickness δ_i of the inner layer can be estimated from several arguments (Belcher & Hunt 1998), all of them giving here nearly the same number. Taking $L = 35\,\mathrm{mm}$ and $y_0 = d/30$, where $d = 0.2\,\mathrm{mm}$ is the grain diameter, the relation (1.1) gives $\delta_i = 2.0\,\mathrm{mm}$. Since the grain roughness is small ($d^+ = 1.9$ for $u_* = 9.45\ \mathrm{mm\,s^{-1}}$), the velocity profile over a smooth wall may be preferred for U_0, which gives the close result $\delta_i = 2.2\,\mathrm{mm}$. A simpler estimation of δ_i arises from the balance of the horizontal advection time $L/U_0(\delta_i)$ and the vertical diffusion time δ_i/u_*; this leads to a relationship very similar to (1.1) (with κ instead of $2\kappa^2$ on the right hand side), and gives $\delta_i = 2.6$ mm. Among the three values above, the intermediate value $\delta_i = 2.2\,\mathrm{mm}$ is retained in the following, for which we note that $U_0(\delta_i) \approx 0.62\,U_\delta$. Two remarks can now be made. First, the peaks of the Lagrangian speed-up ΔU_L and the vertical velocity V occur at $y_d \approx 0.05\,\delta$ (see Figure 8), which correspond to $y_d \approx 0.7\,\delta_i$. Thus, the peak of the speed-up lies in the upper part of the inner layer, which is consistent with the idea that the fluid acceleration over the dune is essentially an inviscid phenomena. Second, $\delta_i = 2.2$ mm corresponds to $\delta_i^+ = 21$

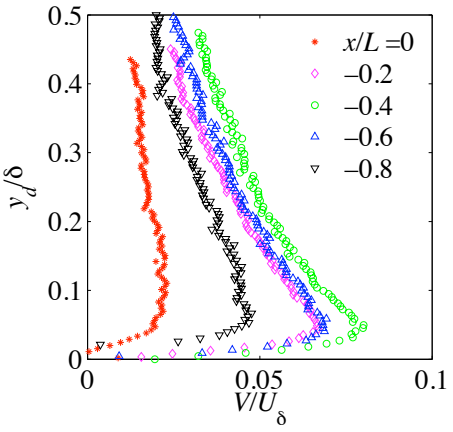

FIGURE 7. Profiles of the vertical velocity V, normalized with U_δ, at five x-positions upstream of the crest ($x/L = 0$). Parameters: see Figure 4.

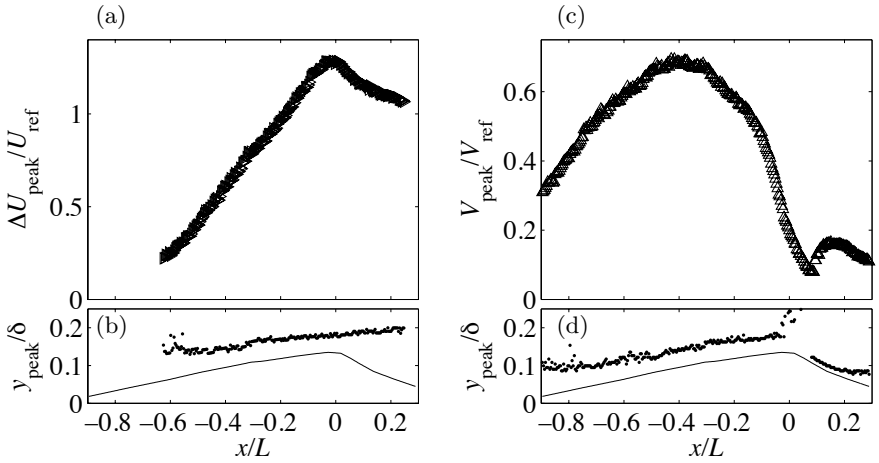

FIGURE 8. (a) Variation along the dune of the peak of the speed-up, $\Delta U_{L,\mathrm{peak}}$, normalised with $U_{\mathrm{ref}} = (H/\delta)U_\delta$; (b) vertical position of $\Delta U_{L,\mathrm{peak}}$ (dots) and the dune profile for reference. (c) and (d), Same for the peak of the vertical velocity, V_{peak}, normalised with $V_{\mathrm{ref}} = (H/L)U_\delta$. Parameters: see Figure 4.

in wall units, so that viscous effects are expected to play a significant role in the inner layer.

The measured velocity field in the outer layer ($y_d > \delta_i$) may be compared to the results of the asymptotic analysis of Hunt *et al.* (1988). However, these results hardly apply here, since (i) there is no upper irrotational layer in channel flows, and (ii) there is no middle layer with zero vertical pressure gradient as will be shown below. Moreover, the analysis of Hunt *et al.* considers unbounded flow in both the vertical and spanwise directions. The existence of an inviscid outer layer may however be assessed using another way, which accounts for the geometrical complications of the present flow (finite channel height and

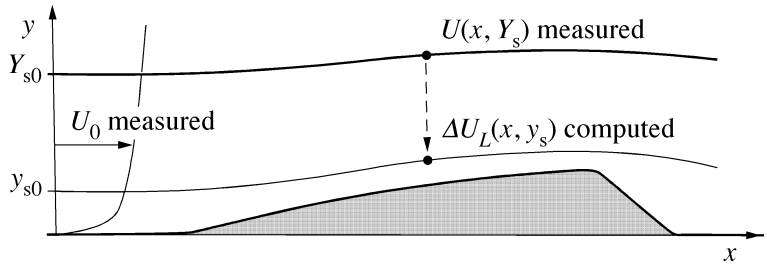

FIGURE 9. Sketch of the determination of the velocity $U(x, y_s)$ from the undisturbed velocity profile $U_0(y)$ and the measured velocity $U(x, Y_s)$ along a single streamline $y = Y_s(x)$ far from the dune.

width) while avoiding its complete calculation. The starting point is to consider that the properties of the perturbed flow are embedded in the variations of the velocity along any particular streamline. Choosing the topmost streamline in the field of view of the camera, given by, say, $y = Y_s(x)$ with $Y_s/\delta \approx 0.5$ (see Figure 9), the pressure perturbation along this streamline is given by the Bernoulli relationship

$$\Delta p_B(x, Y_s) = \frac{1}{2}\rho \left(U_0^2(Y_{s0}) - U^2(x, Y_s) - V^2(x, Y_s) \right), \tag{3.3}$$

where Y_{s0} is the height of the undisturbed streamline upstream of the dune and U and V are the measured velocities. The pressure perturbation Δp_B and velocity U_B along any streamline $y = y_s(x)$ then satisfy the inviscid momentum equations

$$\Delta p_B(x, y_s) = \frac{1}{2}\rho \left(U_0^2(y_{s0}) - U_B^2(x, y_s) \right) \tag{3.4a}$$

$$\Delta p_B(x, y_s) - \Delta p_B(x, Y_s) = -\int_{y_s}^{Y_s} \rho \frac{U_B^2}{R} dy \tag{3.4b}$$

where $R^{-1} = y_s''(1+y_s'^2)^{-3/2}$ is the curvature of the streamline. Taking the streamlines as determined from the velocity measurements, the above equations can be used to determine the pressure perturbation Δp_B and the Lagrangian speed-up $U_B(x, y_s) - U_0(y_{s0})$, as sketched in Figure 9. It has been verified that, due to the small slope of the streamlines, the second-order contribution of the normal velocity V is negligible in (3.4*a*-3.4*b*), so that it is omitted here, and that the integration normal to the streamlines can be safely replaced by the integration along the y-direction. Note that the above procedure cannot be considered as a complete calculation of the perturbed flow since it involves the knowledge of the streamlines of the total flow, but it allows the assumption of inviscid flow to be assessed, as well as that of the existence of a layer with $\partial_y p = 0$.

The resulting prediction of the speed-up is shown in Figure 10, along with the measurements already shown in Figure 6c. It can be seen that in the outer layer (above the dashed-dotted line corresponding to $\delta_i = 2.2\,\mathrm{mm}$), the inviscid calculation (thick lines) matches the experiments quite well. In the inner layer where shear stresses are not negligible, the agreement is poor, as expected. Figure 10 also displays the predicted speed-up when the curvature of the streamlines is ignored, *i.e.* $R = \infty$ in (3.4*b*) or $\partial_y p = 0$ (dashed lines). As expected, this calculation overpredicts the speed-up near the foot of the dunes, since it ignores the retarding effect of the positive curvature associated with larger pressure near the dune than far above. Conversely, the calculation underpredicts the speed-up near the crest since it ignores the acceleration due to the negative curvature and lower pressure.

The above analysis is confirmed by the pressure profiles shown in Figure 11, which

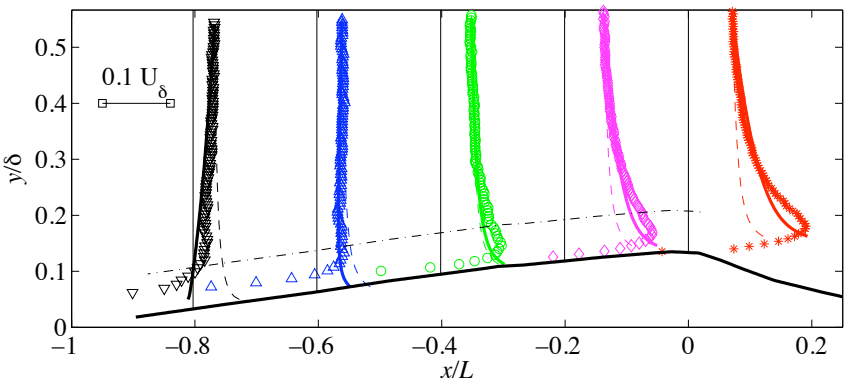

FIGURE 10. Vertical profiles of the Lagrangian speed-up ΔU_L over the dune; (—), inviscid calculation (3.4*a*-3.4*b*); (– –), streamline curvature ignored; (– · –), lower limit of the outer layer with $\delta_i = 2.2\,\mathrm{mm}$. Parameters: see Figure 4.

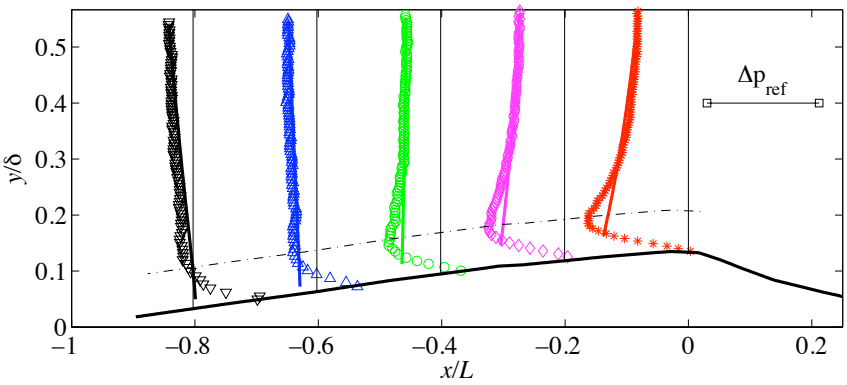

FIGURE 11. Five profiles of the pressure perturbation Δp over the dune; markers, experiments; (—), inviscid calculation (3.4*a*-3.4*b*); (– · –), lower limit of the outer layer with $\delta_i = 2.2\,\mathrm{mm}$. $\Delta p_{\mathrm{ref}} = \rho U_\delta^2 (H/\delta) \approx 4.6\,\mathrm{Pa}$. Parameters: see Figure 4.

shows good correspondence between the pressure perturbation predicted from (3.4) and the measured kinetic energy decrease $\frac{1}{2}\rho(U_0^2 - U^2)$. It appears that the pressure decrease far above the dune ($y/\delta \approx 0.5$), where the streamline curvature is small, is counteracted by the centrifugal effect near the foot of the dune, and enhanced near the crest. Both effects are of the same order of magnitude: the magnitude of the Bernoulli decrease is $\Delta p_{\mathrm{ref}} = \rho U_\delta^2 (H/\delta) \approx 4.6\,\mathrm{Pa}$, while that of centrifugal effect is $\rho U_\delta^2 (\delta/R) \approx 5.7\,\mathrm{Pa}$ (with the streamline curvature R^{-1} estimated from that of the dune profile, $\pi^2 H/4L^2$ according to (2.3)).

3.3. *Analysis in the inner layer*

In the inner layer ($y_d \lesssim \delta_i = 2.2\,\mathrm{mm}$), the vertical profiles of the speed-up exhibit a peak below which the speed-up decreases to zero at the dune surface, as discussed briefly in the previous section (see Figure 10). In this layer, the effect of the Reynolds stresses on the

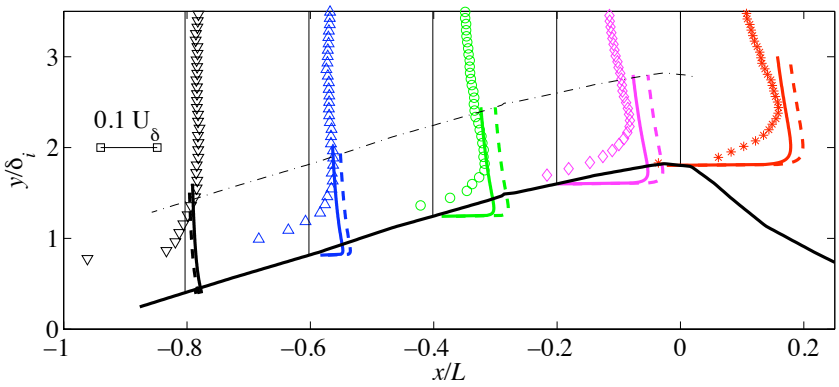

FIGURE 12. Vertical profiles of the measured speed-up ΔU_L (markers), and comparison with the inner layer calculations by Hunt *et al.* (1988). (—), bell-shaped dune $h_M/(1+(x/L)^2)$; (– –), Gaussian dune $h_M\ \exp(-(x/L)^2)$; (– · –), upper boundary of the inner layer with $\delta_i = 2.2\,\mathrm{mm}$. Parameters: see Figure 4.

dynamics of the flow perturbation is no longer negligible as discussed in the Introduction Section, and since $\delta_i^+ = \delta_i u_*/\nu = 21$ is not large, viscosity is expected to play some role as well.

A solution is given by Jackson and Hunt (1975) for a symmetric hill with shape $h_M/(1+(x/L)^2)$ (their eqs. (3.16) and (3.17)). The predicted speed-up (not shown) increases monotonically with height within the inner layer (no peak); it increases along the dune profile too, reaching, with the parameters of the present experiment, the value $\Delta U \approx 0.9\,U_\delta$ at the crest (at $y = \delta_i$). This value is larger than the measured speed-up peak by a factor four. From the improved analysis by Hunt *et al.* (1988) and their solution for a sinusoidal hill (their eq. (3.7)), the flows over two symmetric dune profiles have been computed, using Fourier transforms: the bell profile $h_M/(1+(x/L)^2)$ and the Gaussian profile $h_M\ \exp(-(x/L)^2)$ (see the Appendix for details). The resulting speed-up is shown in Figure 12. It can be seen that the agreement with the measurements is not very good, for both dune profiles: although the value of the peak is not far from that measured (the agreement might be improved by the matching with the measured speed-up inherited from the outer layer), the peak is located very close to the dune surface, where the speed-up consequently exhibits very large velocity gradient. Note that the no-slip condition at the dune surface is not accounted for by the solution in the inner layer, but by the matching with the solution in a very thin surface layer (the fourth layer of the model) with thickness of the order of the roughness length (here a fraction of the grain diameter).

The failure of the above predictions is likely to be due to viscous effects since the thickness of the inner layer, in wall units, is only $\delta_i^+ = 21$. This can be seen by considering the velocity gradient $U'(y)$, whose vertical profiles are shown in Figure 13 at the same five longitudinal locations as before. With u_*^2/ν chosen as the normalization scale, a velocity gradient equal to unity at the dune surface corresponds to shear stress equal to ρu_*^2, *i.e.* the shear stress on the smooth channel wall. It can be seen that all profiles are similar, showing that the velocity gradient increases as the dune surface is approched, approximately linearly for $y_d^+ \lesssim 10$ as for viscous Poiseuille flow. The value reached at the dune surface is about twice that on the smooth wall. This point is discussed further in the next section devoted to stresses.

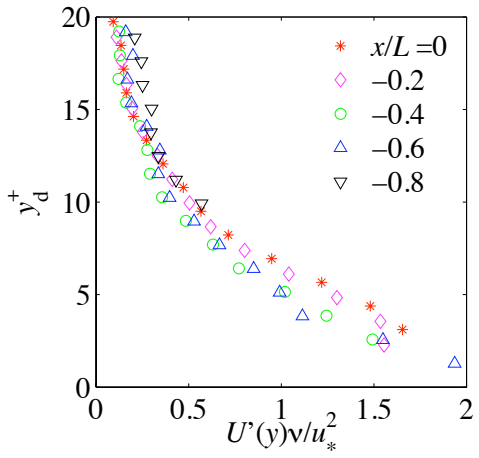

FIGURE 13. Vertical profiles of the mean velocity gradient dU/dy in the inner layer ($y_d^+ < \delta_i^+ = 21$), at five x-positions upstream of the dune crest. Parameters: see Figure 4.

The linear variation of the velocity gradient suggests the search of a parabolic fit of the velocity profiles, of the form $ay_d^2 + by_d$ (the following development was inspired by the Stratford method for the determination of the separation point in an boundary layer, see Schlichting & Gersten (2000)). The constants a and b have been chosen such that the parabola joins smoothly the outer flow $U_B(x, y_s)$ along a particular streamline $y_s(x)$ close to $y_d = \delta_i$, that is

$$ay_s^2 = U_B'(x, y_s)y_s - U_B(x, y_s), \qquad by_s = 2U_B(x, y_s) - U_B'(x, y_s)y_s. \tag{3.5}$$

The result is shown in Figure 14. It can be seen that the composite profiles fit nicely all the measurements over the whole height of the flow. It appeared however that the slope of the profile at the dune surface (*i.e.* the shear stress acting on the dune) was sensitive to the choice of the streamline chosen for the matching. This streamline –the dotted line in the Figure– was chosen in order to fit the shear stress at the dune surface (see the next section). It is noteworthy that the 'effective pressure gradient' $2\mu a$ resulting from the fitting procedure is much smaller than the actual pressure gradient found at the edge of the outer layer from the Bernoulli calculation: the 'effective pressure gradient' decreases from $-0.3\,\Delta p_{\rm ref}/L$ near the foot of the dune to $-0.9\,\Delta p_{\rm ref}/L$ at the crest, where $\Delta p_{\rm ref} = \rho U_\delta^2 (H/\delta) \approx 4.6\,$Pa, whereas the actual pressure gradient is nearly uniform with value $-0.9\,\Delta p_{\rm ref}/L$. The difference between the actual and 'effective' pressure gradients corresponds to the acceleration of the flow, which thus represents 2/3 of the pressure gradient near the dune foot, and zero near the crest.

4. Stresses

4.1. *Reynolds stresses*

The determination of the Reynolds stresses along the dune requires the calculation of the momentum transfer across the streamlines of the mean flow. Let u' and v' be the velocity fluctuations in the cartesian plane, and u_s and v_s the fluctuations in the curvilinear coordinate system made of the streamlines, with local angle $\alpha(x, y)$, as sketched in Figure 15. In the curvilinear system, the transverse mean velocity V_s is zero and the turbulent

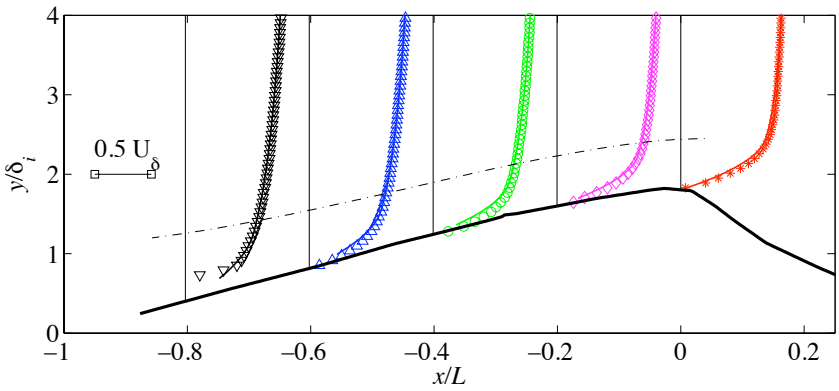

FIGURE 14. Measured velocity profiles (markers) and composite fits (solid lines); (– · –), streamline on which the matching of the outer Bernoulli calculation and the inner parabolic fit is performed. Parameters: see Figure 4.

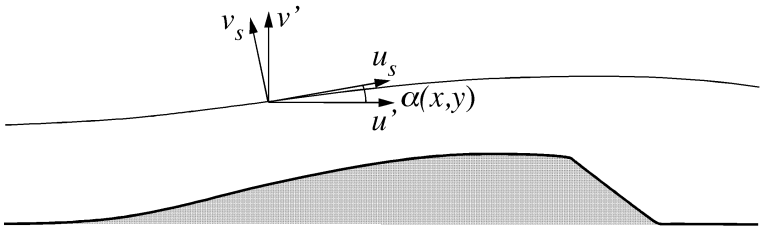

FIGURE 15. Sketch of the velocity fluctuations in the cartesian coordinate system, u and v, and following the streamlines, u_s and v_s.

shear stress are

$$\overline{(U_s+u_s)(V_s+v_s)} = \overline{u_s v_s}$$
$$= \overline{u'v'}\cos 2\alpha - \frac{1}{2}(\overline{u'^2} - \overline{v'^2})\sin 2\alpha, \qquad (4.1)$$

where the angle $\alpha(x,y)$ is obtained from $\tan\alpha = V/U$. The normal stresses $\overline{u_s^2}$ and $\overline{v_s^2}$ in the local reference frame can be computed from similar relations.

Figure 16a displays vertical profiles of the normal Reynolds stress $\overline{u_s^2}/u_*^2$ at five positions upstream of the crest (where u_* is the friction velocity on the smooth wall, as before). At all the longitudinal positions, this stress increases towards the dune surface in the outer layer ($y_d \gtrsim \delta_i = 0.07\,\delta$), as expected, reaches a maximum at $y_d \approx \delta_i$, of 4–5 u_*^2, and then decreases to zero in the inner layer. The vertical location of the peak slightly lowers as the dune crest is approached, from $y_d \approx 0.07\,\delta$ down to $y_d \approx 0.04\,\delta$, which effect is partly due, at least, to the compression of the streamlines. At a given height above the dune (fixed y_d), $\overline{u_s^2}$ clearly decreases towards the crest. The relative decrease $\Delta\overline{u_s^2}/\overline{u_s^2}$ is large, of about 50%, or, in terms of the dimensionless speed-up, of about $-3\,\Delta U_L/U_\delta$. This decrease of $\overline{u_s^2}$ in a region where the flow is accelerated is consistent with the rapid distortion (Davidson 2004). Similar observations were made by Gong *et al.* (1996) for the boundary layer flow over a sinusoidal rough wall, with however a smaller decrease of about 25% (over the first wave where the flow can be expected to respond as on a single wave).

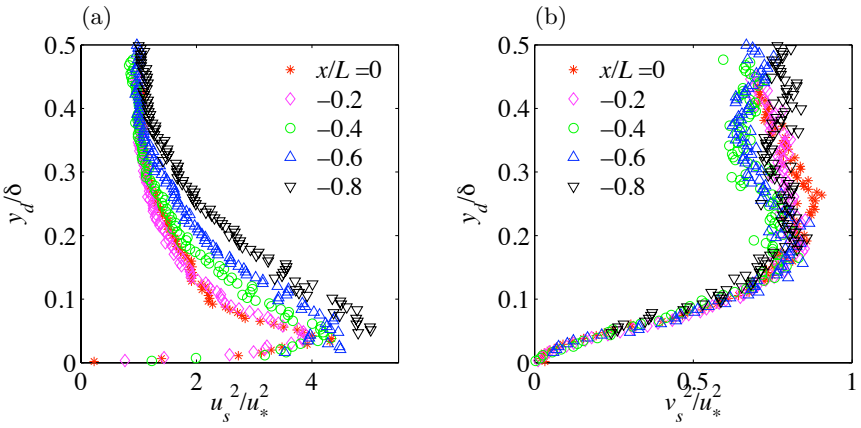

FIGURE 16. Vertical profiles of the normal Reynolds stresses normalized with u_*^2, at five positions upstream of the crest; (a) $\overline{u_s^2}$; (b) $\overline{v_s^2}$. Parameters: see Figure 4.

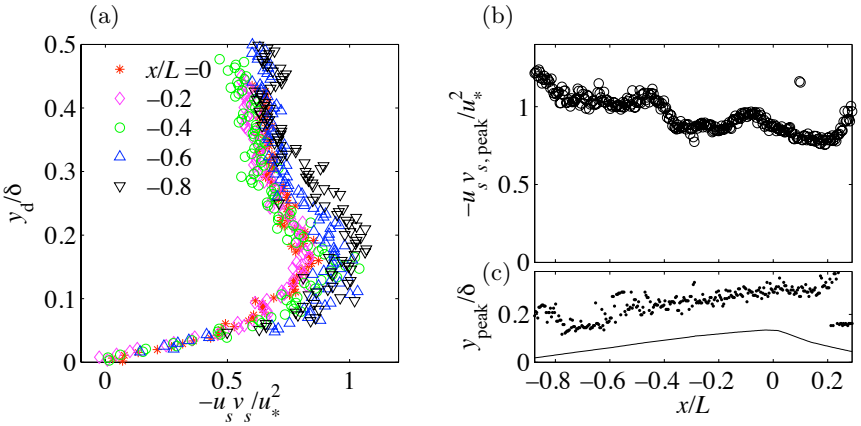

FIGURE 17. (a) Vertical profiles of the Reynolds shear stress $-\overline{u_s v_s}$, normalized with u_*^2, at five positions upstream of the crest. (b) Variation along the dune of the value of the peak. (c) Variation along the dune of the vertical location of the peak. Parameters: see Figure 4.

Figure 16b displays profiles of the normal stress $\overline{v_s^2}$. At all the longitudinal locations, this stress first increases towards the dune surface, reaches a maximum of $0.8\,u_*^2$ at $y_d \approx 0.2\,\delta$, and then decreases monotically in the inner layer. The variations along the dune are quite small, with no clear trend.

Figure 17a displays the profiles of the Reynolds stress $-\overline{u_s v_s}$. These profiles are similar to those over the smooth wall (note that $-\overline{u_s v_s}$ remains positive near the dune surface, whereas $-\overline{u'v'}$ in the cartesian plane exhibits negative values there). In particular, they exhibit a smooth peak at the location $y_d \approx 0.2\,\delta \approx 3\,\delta_i$. The variation along the dune of the peak value and its vertical location are plotted in Figures 17b and 17c, respectively;

although the measurements exhibit some scatter, the peak value clearly decreases by about 25%, from $1.1\,u_*^2$ at the dune foot to $0.8\,u_*^2$ at the crest, approximately.

To summarize, the normal stress $\overline{u_s^2}$ was found to decrease along the dune, by about u_*^2. This decrease is however small in comparison with that of pressure, which is proportional to the decrease of U^2 from the previous analysis, and can be estimated as $2U_0(\delta_i)\Delta U_{L,\mathrm{peak}} \approx 80\,u_*^2$. No significant variation of $\overline{v_s^2}$ was noted. The variations of the shear stress $-\overline{u_s v_s}$ are significant in the inner layer only, and there in the vertical direction only. Finally, it can be concluded that the longitudinal gradient of the Reynolds stresses is negligible in the whole flow, in comparison with that of pressure. Their vertical gradient is negligible as well, except for that of the shear stress in the inner layer. The magnitude of the latter, $-\partial_y \overline{u_s v_s} \approx u_*^2/\delta_i \approx 16\,u_*^2/L$, is comparable to the longitudinal gradient of pressure, $\partial_x p \approx 80\,u_*^2/L$. The difference between these gradients results in fluid acceleration in the inner layer.

4.2. *Mixing length*

As shown in Section 3.3, the asymptotic analysis of Hunt *et al.* (1988) fails to predict the observed velocity profile in the inner layer, and since $\delta_i^+ = 21$, the probable reason for this failure was attributed to viscous effects. This reason may be confirmed by assessing the crucial assumption that the Reynolds shear stress can be modelled with the mixing length theory,

$$-\overline{u_s v_s} = \ell^2 \left(\frac{dU}{dy}\right)^2 \tag{4.2}$$

with $\ell = \kappa y_d$. The length ℓ defined by the above relation can be determined from the measured Reynolds stress and mean velocity gradient. Figure 18 displays the result. Were the classical mixing length theory be valid, the length ℓ would increase linearly with height, as κy_d. In fact, Figure 18 shows that for $y_d \lesssim 0.5\,\delta_i$, *i.e.* $y_d^+ \lesssim 10$, the mixing length is nearly zero. For $y_d^+ \gtrsim 10$, it does increase approximately linearly, as $\ell^+ = \kappa(y_d^+ - 10)$ near the foot of the dune, and more strongly as the dune crest is approached, as $\ell^+ = 2\kappa(y_d^+ - 10)$ at the crest. It can be concluded that near the dune foot, the mixing length theory accounts for the relation between the Reynolds stresses and the mean velocity gradient, but above the elevation $y_d^+ \approx 10$ only, *i.e.* outside the viscous sublayer (which is not surprising); as the dune crest is approached, the linear increase of ℓ^+ is stronger than the classical one, by a factor two at the crest.

4.3. *Total shear stress*

The total shear stress along a streamline is the sum of the Reynolds stress and the viscous stress,

$$-\rho\overline{u_s v_s} + \mu\frac{\partial U}{\partial y} \tag{4.3}$$

(it has been verified that the contribution of the neglected terms, of second-order in the small slope α of the streamlines, are effectively negligible). Figure 19a displays vertical profiles of this shear stress. In the outer layer and the upper-half of the inner layer ($y_d \gtrsim 0.5\,\delta_i$ or $y_d^+ \gtrsim 10$), the viscous stresses are negligible (the mean velocity gradient is small) so that the total stress decreases as the Reynolds stress displayed in Figure 17a. Closer to the dune surface, $y_d^+ \lesssim 10$, it can be seen that the total stress increases strongly, approximately linearly: whereas the turbulent stress vanishes, the viscous stress becomes large as the gradient of the mean velocity (see Figure 13).

The actual shear stress τ_d acting at the dune surface can be obtained from the extrapolation of the profiles of the total shear stress. It is shown in Figure 19b (circles): it

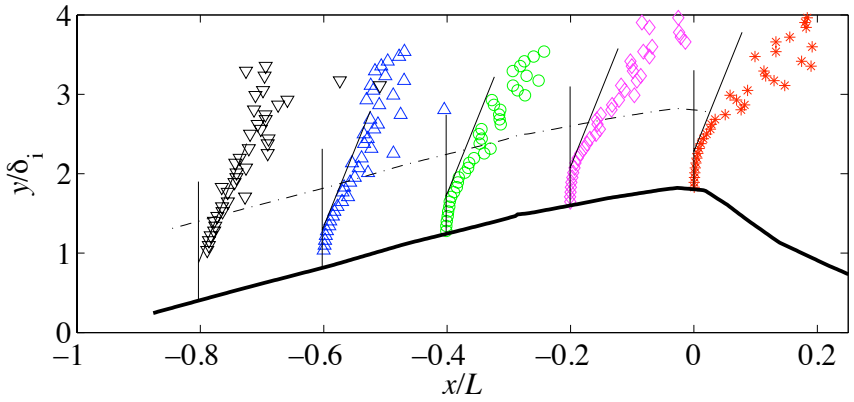

FIGURE 18. Vertical profiles of the mixing length ℓ determined from (4.2), with the measured Reynolds stress and mean velocity gradient; (—), $\ell^+ = \kappa(y_d^+ - 10)$; (– · –), upper limit of the inner layer. Parameters: see Figure 4.

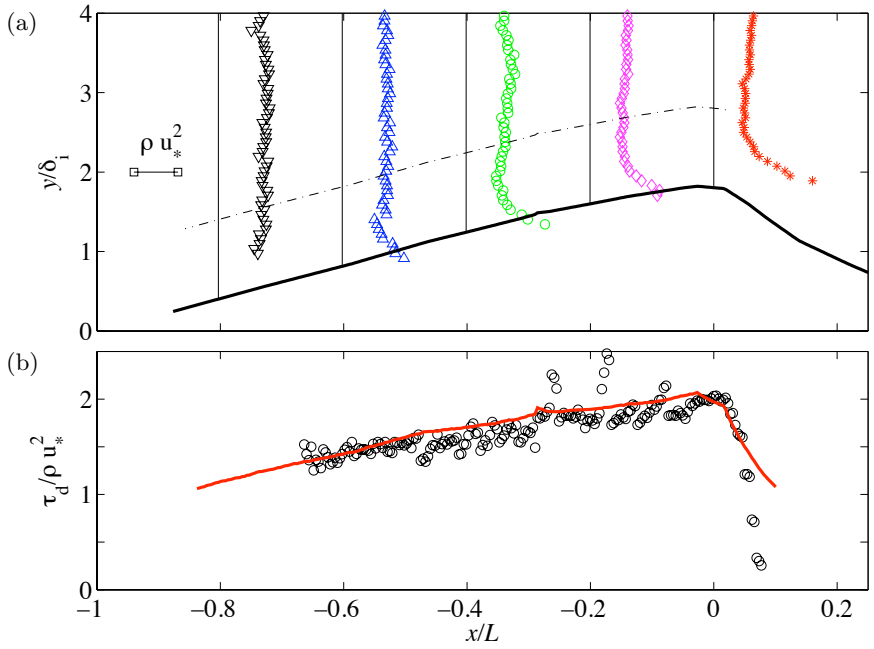

FIGURE 19. (a) Vertical profiles of the shear stress (turbulent and viscous) above the dune; (– · –), upper limit of the inner layer. (b) (○), measured shear stress extrapolated down to the dune surface; (—), shear stress from the parabolic fit of the mean velocity profile with coefficients given by (3.5). Parameters: see Figure 4.

appears that τ_d increases approximately linearly along the dune, and reaches its maximum value, about $2\rho u_*^2$, at the dune crest. Beyond the crest, the shear stress strongly decreases, as expected. The shear stress μb derived from the parabolic fit of the inner velocity, with coefficients (3.5), is also shown in the figure (solid line). The agreement with the measurements is remarkable. Although the streamline on which the matching of

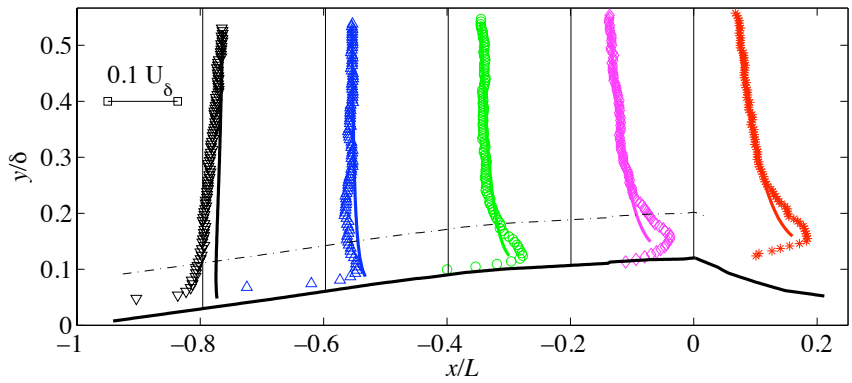

FIGURE 20. Profiles of the Lagrangian speed-up ΔU_L over the dune; (—), Bernoulli prediction with the streamline curvature included; (– · –), upper limit of the inner layer (1.1). $Re = 14300$, $L = 42\,\text{mm}$, $H = 3.6\,\text{mm}$.

the inner and outer flows is performed (see Figure 14) has been chosen in order to achieve this agreement, a good fit over the whole dune profile was not *a priori* guaranteed.

It is noteworthy that the maximum shear stress is reached at the dune brink, whereas theoretical analyses predict that it is reached upstream of the crest of a gentle bump (Benjamin 1959; Hunt *et al.* 1988). This difference may correspond to the fact that the dunes considered here are not smooth surfaces but exhibit a sharp brink where the dune slope is positive (the brink is located upstream of the summit of their cosine envelope, see §2.3). Numerical calculations of the flow above a 'broken' dune may confirm this conjecture.

Finally, the main conclusion of this section is that whereas the peak of the turbulent stress decreases towards the dune crest (Figure 17b), the shear stress at the dune surface increases and reaches its maximum at the dune crest, where it is about twice that of the unperturbed flow on the smooth wall.

5. Variations with the flow velocity

All the results discussed above are for the same Reynolds number, $Re = 9300$, for which the shear stress on the dune was below the threshold for particle motion, so that the dune was at rest. Similar measurements have been performed for Reynolds numbers above the threshold, *i.e.* for moving dunes. These measurements showed essentially the same results. In all cases, the flow is accelerated in the outer layer, whereas in the inner layer the velocity first decreases near the foot of the dune (negative speed-up) and then increases. A peak in the speed-up always develops in the inner layer. As an illustration, Figures 20-22 displays the measured Lagrangian speed-up ΔU_L for $Re = 14300$, 16200 and 18300. From the lowest to the highest Reynolds number, the thickness of the inner layer decreases slightly from $\delta_i = 2.2\,\text{mm}$ to $\delta_i = 2.0\,\text{mm}$. In all cases, the inviscid calculation (3.4) provides a good representation of the flow in the outer layer, as shown by the solid lines in Figures 20-22.

The variation along the dune of the peak of the speed-up and the peak of the vertical velocity are shown in Figure 23. The maximum speed-up always occurs at the dune crest (Figure 23a); no upstream shift of this maximum is visible. This maximum is in the

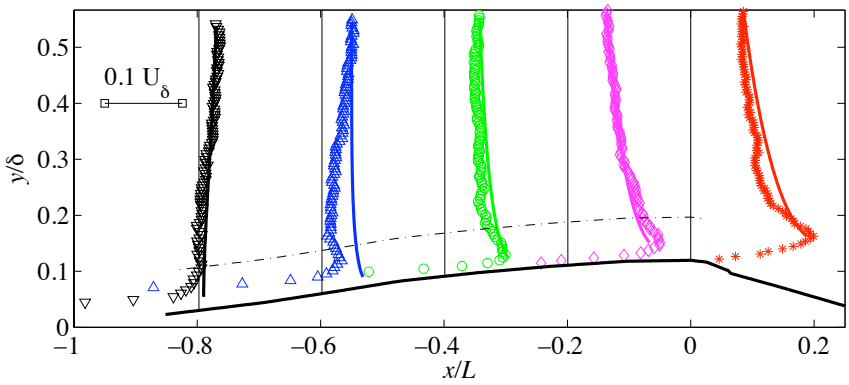

FIGURE 21. Same as Figure 20 for $Re = 16200$, with $L = 40\,\mathrm{mm}$, $H = 3.6\,\mathrm{mm}$.

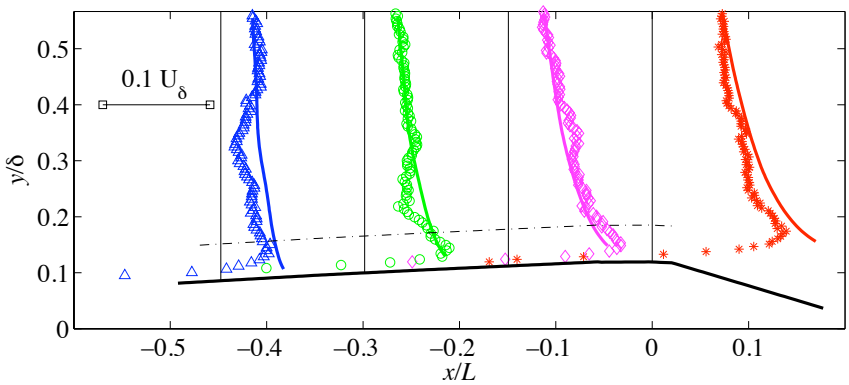

FIGURE 22. Same as Figure 20 for $Re = 18800$, with $L = 34\,\mathrm{mm}$, $H = 3.6\,\mathrm{mm}$.

range 1–1.4 U_{ref} where $U_{\mathrm{ref}} = (H/\delta)U_\delta$ is the expected order of magnitude. Except for $Re = 9300$ where the dune is at rest, the maximum speed-up decreases with increasing Reynolds number. Turning to the vertical velocity, Figure 23b shows that its maximum is in the range $0.7 - 1$ and occurs approximately at the middle of the upstream face.

Figure 24 displays the variation along the dune of the peak of the normalized turbulent shear stress, for the same four Reynolds numbers and dunes as in Figure 23. These measurements exhibited some scatter, which may be induced by the slow motion of the dune, or by three-dimensional flow structures related to the lateral meandering of the streaks observed at the dune surface (see Part One). A running average over a few points has been performed in order to make more visible the variations along the dune: for all Reynolds numbers, the peak of the turbulent shear stress can be seen to decrease slightly towards the crest, from $1.2\,u_*^2$ to $1.0\,u_*^2$ approximately.

Finally, Figure 25 displays the normalized shear stress on the dune, obtained as in Figure 19b from an extrapolation down to the dune surface of the mean velocity gradient in the lower part of the inner layer. For the smallest Reynolds number (for which the dune was at rest), the shear stress increases slightly towards the crest, as noted in the previous

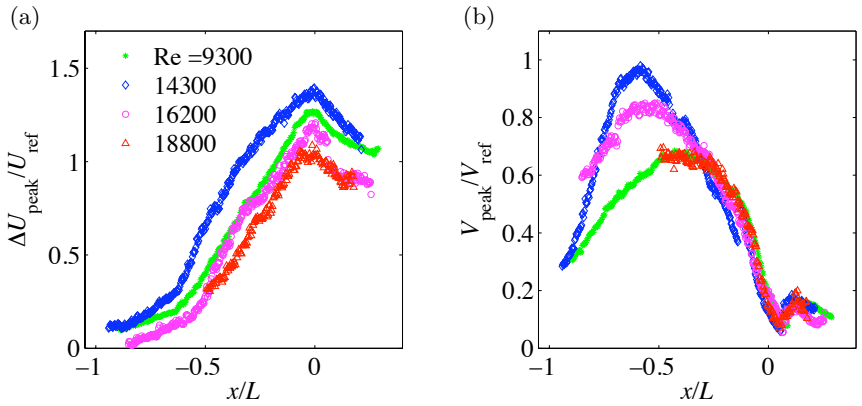

FIGURE 23. Variation along the dune, for four Reynolds numbers, of (a) the peak $\Delta U_{L,\mathrm{peak}}$ of the speed-up normalized by $U_{\mathrm{ref}} = (H/\delta)U_\delta$, and (b) the peak V_{peak} of the vertical mean velocity normalized by $V_{\mathrm{ref}} = (H/L)U_\delta$. For the dune lengths and heights, see Figures 4 and 20-22.

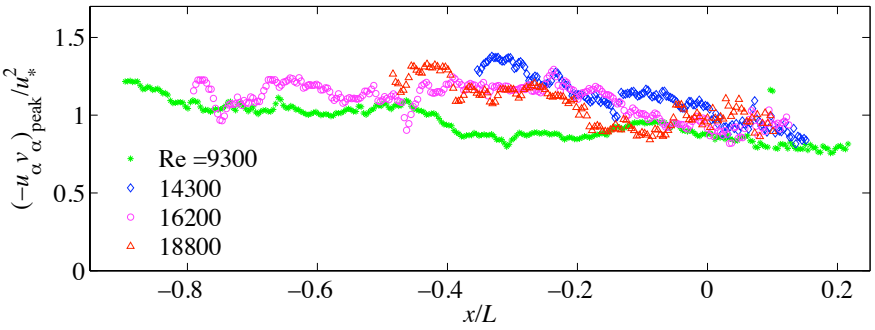

FIGURE 24. Variation along the dune of the peak of the normalized turbulent shear stress $-\overline{u_s v_s}$, for four Reynolds numbers and the same dunes as in Figure 23.

section. For the three larger Reynolds number for which the dune was moving, the increase is less evident. However, a variation with the Reynolds number clearly appears: the normalized shear stress decreases as the Reynolds number increases, from $2.0\,\rho u_*^2$ for $Re = 9300$ down to $1.5\,\rho u_*^2$ for $Re = 18800$. The reason for this decrease may be related to a relaxation of the fluid flow induced by the grain motion. Investigations of the flow over fixed dunes would clarify this point.

6. Summary and discussion

The results presented in this paper of the flow above a barchan dune in a channel can be summarized as follows:

• The fluid flow accelerates along the dune. A peak develops in the vertical profiles of the speed-up, located in the upper part of the inner layer. The Lagrangian speed-up, *i.e.* the actual velocity variation of the fluid particles, is significantly smaller than the 'same-elevation' speed-up considered in theoretical analyses –of about one-half–. The maximum speed-up is reached at the dune brink, where it is of about $1.3\,(H/\delta)U_\delta$; for some fluid

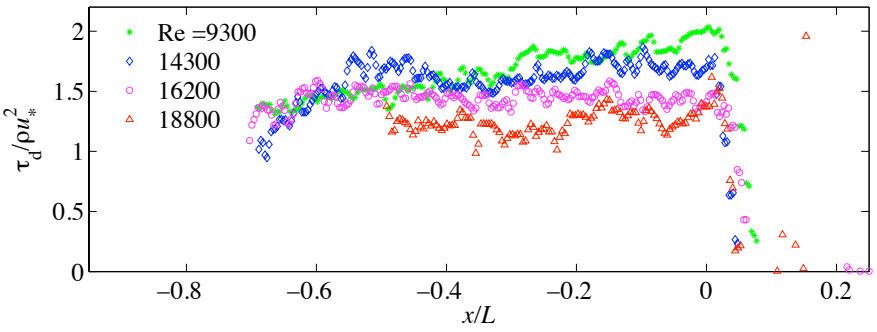

FIGURE 25. Variation along the dune of the normalized shear stress $\tau_d/\rho u_*^2$ at the dune surface, for four Reynolds numbers and the same dunes as in Figure 23.

particles, the speed-up may reach 40% of their upstream velocity. The vertical velocity is maximum at mid-slope, where it is of about $0.7\,(H/L)U_\delta$.

• The fluid flow has a two-layer structure, as predicted by asymptotic analysis: a viscous (turbulent) inner layer with thickness δ_i, and an inviscid outer layer. In the outer layer, the effect of streamline curvature is of the same order of magnitude as the Bernoulli effect related to the compression of the streamlines: it inhibits the speed-up near the foot of the dune and enhances it near the crest; in other words, ignoring the transverse pressure gradient (as in the boundary layer equations) leads to an underestimate of the speed-up by a factor two. This result contrasts with that of Poggi *et al.* (2007) for the flow over sinusoidal waves with small slope ($kh_M \approx 0.078$), where the pressure gradient was shown to be hydrostatic. In the inner layer, the analysis of Hunt *et al.* (1988) fails to predict the right flow, perhaps because of viscous effects. Alternatively, we showed that a parabolic fit, matched with the outer velocity, provides a good description of the entire flow. This fit shows that, near the dune foot, the pressure gradient inherited from the outer layer is balanced for one-third by the shear stress, and for two-third by the fluid acceleration; near the crest, shear stress dominates.

• The Reynolds stresses have been determined in the reference frame of the streamlines. Their vertical profiles are similar to those over a flat wall, with a well-defined peak. $\overline{u_s^2}$ decreases slightly along the dune, whereas $\overline{v_s^2}$ remains constant. The peak of $-\overline{u_s v_s}$, which is located in the outer layer, decreases by about 25% along the dune, from $1.1\,u_*^2$ at the dune foot to $0.8\,u_*^2$ at the crest. The mixing length ℓ is zero within the viscous sublayer (which was half of the thickness of the outer layer for the lower Reynolds number); outside the viscous sublayer, it increases linearly with height, with the usual slope κ near the dune foot but larger slope 2κ near the crest. In the outer layer, the gradient of the Reynolds stresses is negligible compared to that of pressure; in the inner layer, only the vertical gradient of the shear stress is significant. These results support the hypotheses of asymptotic analyses, except for the increase of the mixing length with height, which is stronger by a factor two, near the crest, as compared to Prandtl theory.

• The total stress, viscous and turbulent, increases strongly in the lower part of the inner layer where the viscous stresses dominate. At the dune surface, the total shear stress increases towards the crest; there, it reaches $2\rho u_*^2$, *i.e.* twice its value on the smooth wall. This value is comparable with asymptotic and numerical results for large aeolian dunes (Weng *et al.* 1991; Kroy *et al.* 2002). The maximum shear stress was reached at the brink, not upstream; this observation does not contradict the well-known result that over a

gentle bump, without flow separation, the maximum shear stress is attained upstream of the crest, because of fluid inertia (see the introductory section). Our observation indicates that, at least when the brink is located upstream of the summit of the dune envelope, the slip face and flow separation play an important role in the distribution of shear stress (consistently with the theory of boundary-layer separation (Batchelor 1967; Schlichting & Gersten 2000)). Thus, flow calculations replacing the dune and the recirculation bubble by a smooth envelope must be considered with caution, as noted by Kroy *et al.* (2002); for barchan dunes, three-dimensional effects might also be of importance.

- The above results were for the lowest Reynolds number $Re = 9300$ for which the dune was at rest. They hold for higher Reynolds number, for which the dune was moving. Weak dependences with Re were however found: doubling Re, the normalized maximum speed-up and vertical velocity decrease by 30%; the normalized surface shear stress decreases by 30% too. This decrease might be related to the decreasing importance of viscosity, or to the increasing particle motion; experiments on fixed dunes would clarify this point.

Finally, the investigation of the water flow above an isolated dune allows detailed assessment of asymptotic analyses. Such an assessment is much easier than for large aeolian dunes, for which the flow conditions can hardly be controlled. Some important questions remain however unanswered, such that the structure of the flow near the horns (which controls the small particle leak), the relationship between the surface shear stress and the particle flux (which controls the dune velocity and stability), or the effect of the fluid streaks reported in the Part One of this study. These questions are left for future work.

We thank John Hinch and Paolo Luchini for stimulating discussions and helpful suggestions. We also thank S. Cazin for valuable technical help. We are grateful to the French Agence Nationale de la Recherche for partial financial support of this study (#ANR-07-BLAN-0180-01), and to the Brazilian government foundation CAPES for the scholarship grant of E. M. Franklin.

Appendix A. Flow in the inner layer after Hunt *et al.* (1988)

In this appendix we summarize the asymptotic analysis of Hunt *et al.* (1988) and discuss its application to channel flow. Consider the turbulent flow over a dune of length L and height $H \ll L$, with profile $h(x) = Hf(x/L)$ and roughness y_0. Far upstream of the dune, the unperturbed velocity $U_0(y)$ is logarithmic in the boundary layer of thickness $\delta_{\rm BL}$. Above the dune, the flow can be considered as the superposition of an inner layer where the mixing length theory is assumed to be relevant, and an essentially inviscid outer layer. The thickness δ_i of the inner layer is defined by $(\delta_i/L)\ln(\delta_i/y_0) = 2\kappa^2$.

The outer layer itself is composed of on upper irrotational layer ($y - h(x) \gtrsim \delta_m$) and a middle rotational layer ($y - h(x) \lesssim \delta_m$), where $\delta_m = \delta_{\rm BL}$ for long hills ($L > \delta_{\rm BL}$) and $h_m = L\ln^{-1/2}(L/y_0)$ for shorter hills. The solution in the outer layer provides in particular the pressure $P(x)$ which drives the flow in the inner layer.

In the inner layer, the solution of the linearized problem can be searched as a power series in the parameter $\ln^{-1}(\delta_i/y_0) \ll 1$, such as, for the longitudinal velocity pertubation,

$$\frac{u_d}{U_0(\delta_m)} = \frac{H/L}{U_0(\delta_i)/U_0(\delta_m)}\left(u_d^{(0)}(X,\zeta) + \ln^{-1}(\delta_i/y_0)\,u_d^{(1)}(X,\zeta)\right) \qquad \text{(A 1)}$$

where $X = x/L$, $\zeta = (y - h(x))/\delta_i$ is the normalized vertical distance above the dune,

and $U_0(y) = (u_*/\kappa)\,\ln(y/y_0)$. Taking the Fourier transform in X, *e.g.*

$$u_d^{(0)}(X,\zeta) = \frac{1}{2\pi}\int_{-\infty}^{\infty} \hat{u}_d^{(0)}(k,\zeta)\,\mathrm{e}^{\mathrm{i}kx}\,dk \tag{A 2}$$

the solution for the Fourier components of u_d is found as

$$\hat{u}_d^{(0)} = \hat{\sigma}(k)$$
$$\hat{u}_d^{(1)} = \hat{\sigma}(k)(1 - \log\zeta - 4K_0[2(\mathrm{i}k\zeta)^{1/2}])$$

where K_0 is the modified Bessel function and $-\hat{\sigma}(k) = -k\hat{f}(k)$ is the Fourier transform of the pressure pertubation inherited from the outer layer and normalized with $\rho U_0^2(\delta_m)$. For the bell-shaped dune $f(X) = (1+X^2)^{-1}$, the Fourier transform is $\hat{f}(k) = \pi\,\mathrm{e}^{-|k|}$, and for the Gaussian dune $f(x) = \mathrm{e}^{-X^2}$, it is $\hat{f}(k) = \sqrt{\pi}\,\mathrm{e}^{-k^2/4}$.

The shear stress on the dune is given by

$$\frac{\tau_d}{\rho U_0^2(\delta_m)} = 2\frac{H/L}{(U_0(\delta_i)/U_0(\delta_m))^2}\left(\tau_d^{(0)}(X,\zeta) + \ln^{-1}(\delta_i/y_0)\,\tau_d^{(1)}(X,\zeta)\right) \tag{A 3}$$

with

$$\hat{\tau}_d^{(0)} = \hat{\sigma}(k)$$
$$\hat{\tau}_d^{(1)} = \hat{\sigma}(k)(2\ln k + 4\gamma + 1 + \mathrm{i}\pi)$$

where $\gamma \approx 0.5772$ is the Euler constant.

For the above results to be applied to channel flows, a question arises with the definition of the reference velocity $U_0(\delta_m)$, since there is no irrotational upper layer. Considering that the half-height δ of the channel represents some boundary layer thickness and that the dunes are 'long' in the sense that $L > \delta$, we chose $U_0(\delta_m) = U_\delta$ (the centerline velocity) consistently with the analysis of Hunt *et al.* (1988). Hence the velocity profiles shown in Figure 14. Another choice for $U_0(\delta_m)$ would lead to minor changes. A more accurate asymptotic theory for the pressure-driven flow above dunes in closed channels or pipes remains to be performed.

REFERENCES

Abrams, J. & Hanratty, T. J. 1985 Relaxation effects observed for turbulent flow over a wavy surface. *J. Fluid Mech.* **151**, 443–455.

Andreotti, B., Claudin, Ph. & Douady, S. 2002 Selection of dune shapes and velocities. Part 2: a two-dimensional modelling. *Eur. Phys. J. B* **28**, 341–352.

Belcher, S. E. & Hunt, J. C. R. 1998 Turbulent flow over hills and waves. *Annu. Rev. Fluid Mech.* **30**, 507–538.

Benjamin, T. B. 1959 Shearing flow over a wavy boundary. *J. Fluid Mech.* **6**, 161–205.

Davidson, P. A. 2004 *Turbulence: An Introduction for Scientists and Engineers.* Oxford University Press.

Franklin, E.M. & Charru F. 2011 Subaqueous barchan dunes in turbulent shear flow. Part 1: Dune motion. *J. Fluid Mech.*, to appear.

Gong, W., Taylor, P. A. & Dörnbrack, A. 1996 Turbulent boundary-layer flow over fixed aerodynamically rough two-dimensional sinusoidal waves. *J. Fluid Mech.* **312**, 1–37.

Hunt, J. C. R., Leibovich, S. & Richards, K. J. 1988 Turbulent shear flows over low hills. *Q. J. R. Meteorol. Soc.* **114**, 1435–1470.

Jackson, P. S. & Hunt, J. C. R. 1975 Turbulent wind flow over a low hill. *Q. J. R. Meteorol. Soc.* **101**, 929–955.

Kroy, K., Sauermann, G. & Herrmann, H. J. 2002 Minimal model for aeolian sand dunes. *Phys. Rev. E* **66**, 031302.

Luchini, P. & Charru, F. 2010 The phase lead of shear stress in shallow-water flow over a perturbed bottom. *J. Fluid Mech.* 665, 516–539.

Panton, R. L. 2007 Composite asymptotic expansions and scaling wall turbulence. *Phil. Trans. R. Soc. Lond. A* **365**, 733–754.

Poggi, D., Katul, G. G., Albertson, J. D. & Ridolfi, L. 2007 An experimental investigation of turbulent flow over a hilly surface. *Phys. Fluids* **19**, 036601.

Schlichting, H. & Gesten, K. 2000 *Boundary-Layer Theory.* Springer.

Sykes, R. I. 1980 An asymptotic theory of incompressible turbulent boundary-layer flow over a small hump. *J. Fluid Mech.* **101**, 647–670.

Taylor, P. A., Mason, P. J. & Bradley, E. F. 1987 Boundary-layer flow over low hills. A review. *Boundary-Layer Meteorol.* **39**, 107–132.

Weng, W. S., Hunt, J. C. R., Carruthers, D. J., Warren, A., Wiggs, G. F. S., Livingstone, I. and Castro, I. 1991 Air flow and sand transport over sand-dunes. *Acta Mechanica Suppl.* **2**, 1–22.